Astron. Astrophys. 362, 1–8 (2000)

ASTRONOMY AND ASTROPHYSICS

Comptonization in an accretion disk illuminated by protons

B. Deufel and H.C. Spruit

Max-Planck-Institut für Astrophysik, Karl-Schwarzschild-Strasse 1, 85740 Garching, Germany

Received 17 February 2000 / Accepted 6 June 2000

Abstract. We compute the X-ray spectrum from a cool, optically thick, geometrically thin accretion disk embedded in a hot ion supported torus (or ADAF). Most of the gravitational power is assumed to be dissipated in the torus, where the protons are near their local virial temperature. The protons are slowed down in the accretion disk via Coulomb interactions, producing a hot surface layer with an optical thickness $\tau_{\rm T}$ ≈1–2. The heating of this layer is balanced by cooling through Comptonization of soft photons. The soft photons are produced by the reprocessing (treated in an approximate way) of hard photons penetrating into the cool disk. Solving the energy balance problem of the heated layer together with the Comptonization by a Monte-Carlo simulation, we find X-ray spectra reminiscent of observed spectra of AGN and black hole candidates in their hard states.

Key words: accretion, accretion disks – black hole physics – radiative transfer – scattering – X-rays: galaxies – X-rays: stars

1. Introduction

A variety of models have been invoked to explain the hard X-ray spectra of galactic Black Hole Candidates and AGN. The similarity between the spectra of these classes of sources suggests a common mechanism in spite of a large difference in length and time scales. Inverse Compton scattering of soft photons by energetic electrons is the most likely radiation process, and can explain the spectra for a variety of geometries for the assumed soft photon source and hot electron plasma. The source of soft photons could plausibly be a cool disk, extending outward from an assumed distance $r_{\rm i}$ around the central mass. The hot Comptonizing plasma could either form a cloud around the central mass, or a corona above the cool disk. The simultaneous presence of a cool disk and a hot Comptonizing plasma is clearly indicated in some observations of black hole transients. These components are identifiable in the spectra of such sources in their very high, high and intermediate states (Rutledge et al. 1999). A central hot cloud could be provided physically by an optically thin, radiatively inefficient accretion flow or ADAF (Rees et al. 1982; Narayan & Yi 1994; Narayan et al. 1996). A corona could be magnetically heated (Galeev et al. 1979; di Matteo et al. 1999), with the magnetic field being provided by the cool disk, and the energy input being due to the Keplerian shear in the disk. By adjusting the soft photon flux, the temperature, and the optical depth of the hot plasma, photon spectra can be produced that closely resemble the observations.

The interaction between the hot plasma and the cool disk, either in the ADAF or in the coronal model, is traditionally seen in terms of an exchange of photons. Soft photons from the disk illuminate the hot plasma and gain energy by inverse Compton scattering on the hot electrons. A part of the resulting energetic photons in turn illuminates the cool disk, is absorbed there and reprocessed into a larger number of photons of lower energy. Haardt & Maraschi (1991, 1993) have shown that the energy balance between the hot and cool plasma illuminating each other in this way determines a combination of temperature and optical depth of the hot plasma (the Compton y-parameter), in such a way that spectra with approximately the right slope are produced.

If the hot plasma is due to an ADAF flow, it is in a two-temperature state (Shapiro et al. 1976) with the ions near their local virial temperature, and the electrons at a much lower temperature near 100 keV. If such a hot two-temperature cloud exists near a cool disk, as the observations indicate, it is conceivable that interaction with this cool disk takes place not only by photons, but also by the some fraction of the ions losing their energy by penetrating into the cool disk and slowing down there (‘ion illumination’).

Heating of a neutron star surface by impinging ions has been proposed very early in the history of X-ray astronomy. It was suggested as the cause of X-ray emission by Zel’dovitch & Shakura (1969) and Alme & Wilson (1973) but was subsequently eclipsed by the development of accretion through a cool disk.

The possible importance of the process for disks embedded in a hot corona has been proposed by Spruit (1997) and Spruit & Haardt (2000). In these models, the hot Comptonizing plasma is identified with the thin surface layer on top of the cool disk that is produced by the incident flux of ions. The penetration of the ions into the disk, and the propagation of photons through such a layered structure is a well defined problem. The temperature as

Send offprint requests to: bed@mpa-garching.mpg.de

a function of depth in the layer, and the output spectrum depend only on the temperature and energy flux of the incident ions (and weakly on the local acceleration of gravity). The resulting spectra obtained with an approximate treatment of the radiative transfer (Spruit & Haardt 2000) are promising. The optical depth and temperature of the heated layer are in the right range and produce the right spectral slope and high-energy cutoff, depending only weakly on parameters such as the distance from the central mass and energy flux.

Here, we present more detailed calculations of the process, with a more accurate treatment of the Comptonization process. The interaction between the ion torus and the disk is computed time dependently in a one-dimensional, plane-parallel approximation. For each time step we calculate the energy gain of the electrons slowing down the penetrating hot protons, and their energy loss through Compton cooling of soft blackbody photons, until an equilibrium state is obtained. The density distribution through the region is found from hydrostatic equilibrium. The Comptonization is done by a Monte-Carlo calculation. The result is the Comptonized spectrum at the top of the accretion disk. The production of soft photons by the thermalization of hard photons is not included explicitly but represented by a reprocessing surface at an appropriate depth in the model (see Sect. 3.2 for details).

In Sect. 2 we specify the cool disk model into which the protons penetrate. In Sect. 3 we describe the heating of the electrons at the surface of this disk through Coulomb interactions with the incident protons as well as their cooling by Comptonization in the stratified layer. Sect. 4 presents results and conclusions from these calculations and Sect. 5 gives a discussion and summary.

2. A cool disk inside an ion supported accretion flow

The geometry for the accretion flow we consider here consists of an ion supported advection torus or ADAF (Rees et al. 1982; Narayan & Yi 1994, 1995). This flow is assumed to coexist with an optically thick accretion disk, such that the cool disk extends partly into the hot flow. We do not address the question here how much of an overlap between the two is physically realistic. Since the incident ions loose essentially all their energy once they have entered the cool disk, the overlap region is a significant sink of energy and mass from the ADAF. If it is too wide, these losses might be too high for an ADAF to be sustainable. The distance of the overlap region from the hole is treated as a free parameter of the problem.

The properties of the cool disk depend on its accretion rate. We assume here that a fixed fraction f of the energy release is transported to the accretion disk corona (ADC) above the cold disk. All the angular momentum transport and the accretion take place in the cool disk. This allows us to use a standard thin disk model for the cool disk. In the calculations reported, 95% of the accretion energy is released in the ADC.

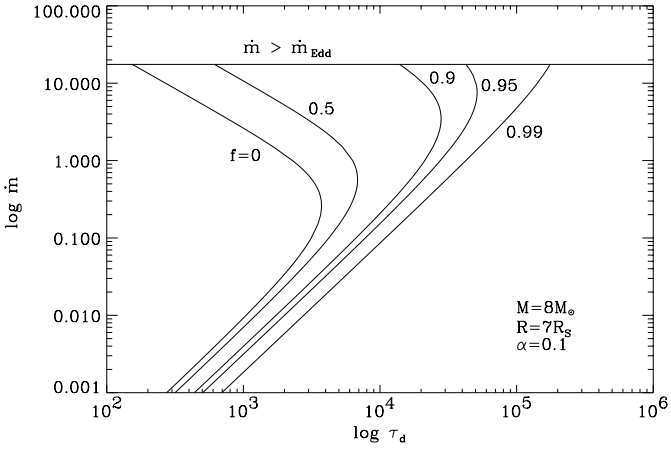

Fig. 1. Disc solutions at a fixed radius $R = 7R_{\rm S}$ from the compact object for various values $f = 0.0, 0.5, 0.9, 0.95, 0.99$, the viscosity parameter $\alpha = 0.1$, and $M = 8M_{\odot}$. The accretion rate is super-Eddington ($\dot{m} > 17.5$ for an accretion efficiency $\eta = 0.057$) above the horizontal line. The transition from the radiation pressure dominated solutions to the gas pressure dominated solutions (break in the curve) moves to higher $\dot{m}$ with increasing f. For $f \approx 1$ only a gas pressure dominated solution exists.

2.1. The radial structure of the cold disk

We set up our cool disk model according to Svensson & Zdziarski (1994) (SZ94). They have shown that if a sufficiently large fraction of the accretion power is dissipated in the accretion disk corona (ADC), a cold, optically thick and pressure supported disk can exist down to small radii very close to the black hole horizon. With increasing f the transition between the gas pressure supported solutions and the radiation pressure supported solutions (corresponding to the break in the curves in Fig. 1) moves to higher $\dot{m}$. The case $f = 0$ represents the standard α disk.

Our solutions of the equations of SZ94 are slightly different, for the gas pressure supported case, because of minor algebraic inaccuracies we detected in SZ94. We present our version of the solutions in Eqs. 1-5. In Fig. 1 we plot the numerical solution for Eq. 28 of SZ94 substituting our result for $\tau_{\rm d,gas}$.

$$\frac{H_{\rm d}}{R} = 2C_1^{-1/10}\left(\alpha_f\frac{m_{\rm p}}{m_{\rm e}}\right)^{-3/10}\left(\frac{R_{\rm S}}{r_{\rm e}}\right)^{-1/10}\times \alpha^{-1/10}r^{-1/20}[\dot{m}J(r)]^{1/5}(1-f)^{1/10} \quad (1)$$

$$\tau_{\rm d} = 2^{-5/2}C_1^{1/5}\left(\alpha_f\frac{m_{\rm p}}{m_{\rm e}}\right)^{3/5}\left(\frac{R_{\rm S}}{r_{\rm e}}\right)^{1/5}\times \alpha^{-4/5}r^{-2/5}[\dot{m}J(r)]^{3/5}(1-f)^{-1/5} \quad (2)$$

$$\rho_{\rm d} = \frac{m_{\rm p}}{\sigma_{\rm T}R_{\rm S}}2^{-7/2}C_1^{3/10}\left(\alpha_f\frac{m_{\rm p}}{m_{\rm e}}\right)^{9/10}\left(\frac{R_{\rm S}}{r_{\rm e}}\right)^{3/10}\times \alpha^{-7/10}r^{-27/20}[\dot{m}J(r)]^{2/5}(1-f)^{-3/10} \quad (3)$$

$$P_{\rm gas,d} = \frac{m_{\rm p}c^2}{\sigma_{\rm T}R_{\rm S}} 2^{-5/2} C_1^{1/10} \left(\alpha_f \frac{m_{\rm p}}{m_{\rm e}}\right)^{3/10} \left(\frac{R_{\rm S}}{r_{\rm e}}\right)^{1/10} \times \alpha^{-9/10} r^{-49/20} [\dot{m} J(r)]^{4/5} (1-f)^{-1/10} \quad (4)$$

$$\frac{k_{\rm B}T_{\rm d}}{m_{\rm e}c^2} = C_1^{-1/5} \alpha_f^{-3/5} \left(\frac{m_{\rm p}}{m_{\rm e}}\right)^{2/5} \left(\frac{R_{\rm S}}{r_{\rm e}}\right)^{-1/5} \times \alpha^{-1/5} r^{-11/10} [\dot{m} J(r)]^{2/5} (1-f)^{2/10}. \quad (5)$$

Here H, τ, ρ, P, T are the pressure scale height, scattering optical depth, mass density, pressure and temperature of the cold disk (subscript d), respectively. We have used the following dimensionless quantities: radius $r = R/R_{\rm S}$, where $R_{\rm S} = 2GM/c^2$ is the Schwarzschild radius of a black hole of mass M, accretion rate $\dot{m} = \eta \dot{M} c^2 / L_{\rm Edd}$, where $L_{\rm Edd} = 4\pi G M m_{\rm p} c/\sigma_{\rm T}$ is the Eddington luminosity and $\eta = 0.057$ denotes the accretion efficiency. α is the standard viscosity parameter according to Shakura & Sunyaev (1973). We have abbreviated $J(r) = 1-(3/r)^{1/2}$ for the inner boundary condition at the inner edge of the disk, α_f is the fine-structure constant, $r_{\rm e}$ is the classical electron radius, $k_{\rm B}$ is the Boltzmann constant, $m_{\rm p}$ and $m_{\rm e}$ are the masses of the proton and the electron, respectively. The numerical value of the coefficient C_1 is given by

$$C_1 = \frac{1024\pi^3}{405\sqrt{2}} = 55.4. \quad (6)$$

2.2. Hydrostatic balance of cool disk and Comptonizing layer

For our calculations we consider the simple idealized case of an accretion disk in a plan-parallel geometry. We assume that the disk and the corona are in hydrostatic equilibrium. The pressure profile $P(\tau)$ as function of optical depth τ is consistently updated throughout our calculation according to the temperature profile $T(\tau)$.

In hydrostatic equilibrium the coronal pressure, $P_{\rm c}$, at the coronal base is in equilibrium with the disk pressure at disk surface, with $P_{\rm c} \ll P_{\rm gas,d}$, the pressure in the mid-plane of the disk. Above this slab we locate the hot protons. A fraction f of the gravitational power $Q(R)$ is assumed to be directly dissipated to the protons. To calculate the pressure that the corona exerts on the top of the disk we have to figure out some numbers first.

The energy exchange between the corona and the disk in our model is mediated by protons only [a model which accounts for the interactions by radiation only was obtained by Haardt & Maraschi (1991; 1993)]. We equal the energy flux by the protons, $q_{\rm p}$, into the cool disk with the viscous energy dissipation in the corona. That is, we neglect both the radiation loss from the corona and energy loss by advection in the corona. These assumptions are for definiteness of the model only, and can easily be generalized.

$$q_{\rm p} = fQ(R) = f \cdot \frac{3GM\dot{M}}{8\pi R^3} \cdot J(R). \quad (7)$$

We assume that the protons above the cool disk have a Maxwellian velocity distribution. This is probably not the case but as the velocity distribution in the corona is not known we consider this assumption to be adequate for our calculations. The energy flux from a Maxwellian proton distribution is given by

$$q_{\rm p} = \frac{1}{2} \frac{m_{\rm p} n_{\rm p}}{\sqrt{\pi}} \left(\frac{2k_{\rm B}T_{\rm p}}{m_{\rm p}}\right)^{3/2}, \quad (8)$$

where $n_{\rm p}$ denotes the number density of the protons. For the temperature of the protons in our model we take the local virial temperature (Rees et al. 1982).

$$T_{\rm p} = T_{\rm vir} = \frac{GMm_{\rm p}}{3k_{\rm B}R} \approx \frac{156}{r} \text{ MeV}. \quad (9)$$

At the distance dominating the energy release, $r \approx 7$, the protons have a temperatures around 20 MeV.

Knowing the proton temperature $T_{\rm p} = T_{\rm vir}$ and the energy flux $q_{\rm p}$ at a certain radius we can calculate the number density $n_{\rm p}$, and with the equation of state the coronal pressure $P_{\rm c}$ of the proton gas at the coronal base, i.e. the surface of the disk:

$$P_{\rm c} = 2\, n_{\rm p} k_{\rm B} T_{\rm p}. \quad (10)$$

As we have assumed a two temperature plasma in the corona with the electron temperature $T_{\rm e} \ll T_{\rm p}$, the contribution to the pressure by the coronal electron gas can be neglected.

$P_{\rm c}$ provides a boundary condition for the pressure at the top of our Comptonizing layer. The height z_0 of this upper boundary above the mid-plane of the disk is not known in advance, but must be found by matching of the Comptonizing layer to the underlying cool disk. The transition between the Comptonizing layer and the cool disk is gradual, and determined by the processes which reprocess the downward flux of hard photons into soft photons. In our calculations this reprocessing is not treated in detail, but replaced by reprocessing into a black body spectrum at an assumed base of the Comptonizing layer, at Thomson depth $\tau_{\rm b}$. The choice of $\tau_{\rm b}$ is discussed in Sect. 3.2.

If $z_{\rm b}$ is the geometric height at $\tau_{\rm b}$, pressure balance between the Comptonizing layer and the underlying cool disk requires that $P(\tau_{\rm b})$=$P_{\rm d}(z_{\rm b})$. If the Comptonizing layer is thin compared with its height above the mid-plane, the acceleration of gravity would be constant and the pressure the layer exerts on the cool disk would be proportional to $\tau_{\rm b}$. In most of our results, the Comptonizing layer is indeed thin, but to be sure we have allowed for arbitrary thickness. The pressure exerted on the cool disk then depends on this thickness since the acceleration of gravity increases with height. The layer thickness in turn depends on its temperature distribution, which varies with time as the cooling and heating processes settle towards equilibrium.

Thus we solve the pressure profile by starting with an initial guess for the height of the disk surface above the mid-plane, z_0, and iterating until we get the right value for which the pressure condition condition at $z_{\rm b}$ is fulfilled. The underlying part of the disk is given by the solutions presented in Sect. 2.1, i.e. it is isothermal with temperature $T_{\rm d}$, the pressure at mid-plane is given by $P_{\rm gas}$ and the scale height is $H_{\rm d}$.

The vertical hydrostatic equilibrium calculated from the top of the disk to the mid-plane yields

$$\frac{\mathrm{d}P}{\mathrm{d}z} = \rho\,\Omega_K^2 z \tag{11}$$

where

$$\Omega_K = \left(\frac{GM}{R^3}\right)^{1/2} \tag{12}$$

is the local Kepler angular velocity.

Together with the equation for the scattering optical depth

$$\frac{\mathrm{d}\tau}{\mathrm{d}z} = \rho\kappa_{\mathrm{es}} \tag{13}$$

one obtains a differential equation describing the pressure profile as a function of optical depth for any temperature profile.

$$\frac{\mathrm{d}^2 P(\tau)}{\mathrm{d}\tau^2}\,P(\tau) = \xi\,T(\tau). \tag{14}$$

Eq. 14 is solved via a forth order Runge-Kutta method. We have abbreviated

$$\xi = \frac{2\,\Omega_K^2 k_{\mathrm{B}}}{\kappa_{\mathrm{es}}^2 m_{\mathrm{p}}} \tag{15}$$

where κ_{es} denotes the electron scattering opacity, which for ionized hydrogen is $\kappa_{\mathrm{es}} \approx 0.40\,\mathrm{cm^2 g^{-1}}$. This calculation is done for each time step to account for the new temperature profile after each cooling/heating step.

3. Heating and cooling processes of the model

3.1. Proton illumination of the accretion disk

As mentioned in Sect. 2.2 we equal the energy flux q_{p} of the protons into the disk with the viscously liberated energy at the radius r (Eq. 7).

Now consider a fast proton from the corona with temperature T_{vir} entering the disk and moving through it on a straight trajectory. This is a valid approximation as the protons do not change their path considerably until the very last scattering, where they have already lost almost all of their energy in excess to the electrons.

In a time $\mathrm{d}t$, such a proton with energy E will lose, through electronic collisions, an amount of energy $\mathrm{d}E$,

$$\frac{\mathrm{d}E}{\mathrm{d}t} = \varepsilon_I(E) n_{\mathrm{e}} v_{\mathrm{p}}, \tag{16}$$

where n_{e} is the electron density of the plasma and v_{p} denotes the velocity of the proton. The stopping power $\varepsilon_I(E)$ of a plasma at temperature T_{e} is taken from the results discussed by Spitzer (1962) and Ryter et al. (1970).

$$\varepsilon_I(E) = \frac{4\pi e^4}{m_{\mathrm{e}} v_{\mathrm{p}}^2}\,\ln\Lambda\,[\psi(x) - x\psi'(x)]. \tag{17}$$

Here $\ln\Lambda = \ln[(3/2e^3)(k_{\mathrm{B}}^3 T_{\mathrm{e}}^3/\pi n_{\mathrm{e}})^{1/2}]$ is the Coulomb logarithm, σ_{T} is the Thomson cross-section, $\psi(x)$ and $\psi'(x)$ are the usual error function and its derivative, θ is the angle between the disk plane and the proton velocity, and $x^2 = (m_{\mathrm{e}} v_{\mathrm{p}}^2/2k_{\mathrm{B}}T_{\mathrm{e}})$ is the proton relative energy. This formula holds for non relativistic electron and proton temperatures.

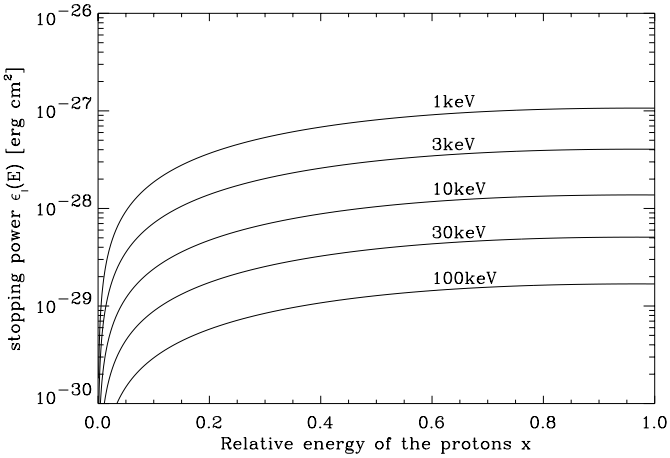

Fig. 2. Stopping power $\varepsilon_I(E)$ vs. proton relative velocity x for different electron temperatures. The electron density is $n_{\mathrm{e}} = 10^{-19}\mathrm{cm}^{-3}$.

The energy deposition of a proton moving at an angle θ with respect to the vertical, per unit of vertical Thomson depth, is

$$\begin{aligned}\frac{\mathrm{d}E}{\mathrm{d}\tau_{\mathrm{T}}} &= \frac{1}{n_{\mathrm{e}}\sigma_{\mathrm{T}} v_{\mathrm{p}}}\frac{1}{\cos\theta}\frac{\mathrm{d}E}{\mathrm{d}t} \\ &= \frac{1}{\sigma_{\mathrm{T}}}\frac{4\pi e^4}{m_{\mathrm{e}} v_{\mathrm{p}}^2\cos\theta}\,\ln\Lambda\,[\psi(x) - x\psi'(x)]\end{aligned} \tag{18}$$

The stopping power of a plasma is plotted in Fig. 2. The stopping power $\varepsilon_I(E)$ decreases with increasing electron temperatures. Once a cold layer is heated by the protons the stopping power of this layer decreases and the protons deposit their kinetic energy in greater optical depths, i.e. they penetrate deeper into the accretion disk. This limits the increase of the electron temperature and is one of the factors which regulates it to a fairly narrow range (the other being the temperature dependence of the Comptonization process). In a steady state the heating by the incident protons is balanced at each depth by the cooling through inverse Compton scattering of soft photons. We calculate the approach to equilibrium of the model in a time dependent way. At each time step the penetration of a Maxwellian distribution of protons of temperature T_{vir} incident on the top of the layer is computed from the temperature $T(\tau)$ and electron density $n_{\mathrm{e}}(\tau)$. This yields the heating rate $f_{\mathrm{p}}^{+}(\tau)$ within the layer.

3.2. Comptonization in a plane parallel disk

The only radiation process explicitly included in our calculations is electron scattering. This is a good approximation in the proton-heated layer, but in the cooler layers below the production of soft photons by bremsstrahlung and atomic processes would have to be considered. Instead, we replace the gradual soft photon production by a complete thermalization at the nominal base τ_{b} of the Comptonizing layer. Thus, at this depth, the down-

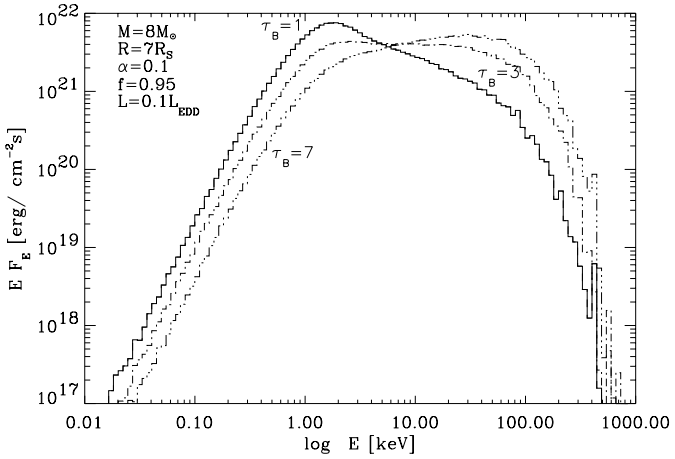

Fig. 3. Spectra for a black hole candidate, as a function of the assumed input depth $\tau_{\rm b}$ of the soft photons. At high $\tau_{\rm b}$ the signature from the blackbody photons completely disappears, whereas at an input depth of $\tau_{\rm b} = 1$ the spectrum is dominated by the soft blackbody bump of unscattered photons.

ward flux $F_{\rm c}^{-}(\tau_{\rm b})$ of (Comptonized) photons is assumed to be converted into a black body flux $F_{\rm BB}^{+}$ of upward soft photons.

Since the results depend somewhat on this thermalizing boundary (see Fig. 3), we need a recipe to get a sensible value for its depth. We do this by computing after each time step the integrated free-free emission $q_{\rm ff}$ over the depth $\tau_{\rm b}$ of the model. Since the thermalizing lower boundary is assumed to represent this gradual photon production, we choose $\tau_{\rm b}$ such that

$$q_{\rm ff} = F_{\rm c}^{-}(\tau_{\rm b}) = F_{\rm BB}^{+}, \tag{19}$$

so that the free-free emission, ignored in the Comptonization calculations, matches the soft photon input $F_{\rm BB}^{+}$ assumed at the base. The free–free luminosity $q_{\rm ff}$ (in erg s^{-1} cm^{-2}) of the layer $\tau_{\rm b}$ (physically extending from z_0 to $z_{\rm b}$) is calculated from the bremsstrahlung emissivity as given by Rybicki and Lightman (1979)

$$q_{\rm ff} = \int_{z_0}^{z_{\rm b}} 1.4\times10^{-27}\, T_{\rm e}^{1/2}\, n_{\rm e}^2\, \bar{g}_{\rm B}\, dz. \tag{20}$$

$\bar{g}_{\rm B}$ is the frequency average of the velocity averaged Gaunt factor, which we set to 1.1. We have thus simplified the gradual thermalization with depth through free–free emission by a step at $\tau_{\rm b}$.

The electron cooling rates through Comptonization in the heated layer are computed through the Monte Carlo method. This also yields the spectrum emitted at the top of the model and the downward flux $F_{\rm c}^{-}(\tau_{\rm b})$ of hard photons incident on the thermalizing boundary, which determines the soft photon input (see Eq. 19).

The method of the Monte Carlo simulation is described in great detail in Pozdnyakov et al. (1983). The algorithms presented there are valid for arbitrary geometries, but rather slow. For speed we have specialized them for use in an inhomogeneous plane parallel medium, i.e. with a one-dimensional stratification of electron densities and temperatures. The density stratification is determined by hydrostatic balance (see Sect. 2.2).

The input photons are created at the lower boundary $\tau_{\rm b}$ with frequency ν_0. The initial photon energy $h\nu_0$ is selected from a blackbody distribution with a temperature obtained from Eq. 19. To each photon we assign a statistical weight w. The photons are emitted isotropically into the upper half space starting with the weight $w_0 = 1$ (Pozdnyakov et al. 1983). The optical depth τ_ν along the trajectory of the photon of frequency ν to the upper/lower boundary of the slab is

$$\tau_\nu = \int_0^{l_\infty} n_{\rm e}(\boldsymbol{r})\, \langle \sigma_\nu(T_{\rm e}, \boldsymbol{r})\rangle\, d\boldsymbol{r} \tag{21}$$

where l_∞ is the physical distance to the corresponding boundary, $n_{\rm e}(\boldsymbol{r})$ is the local electron density and $\langle \sigma_\nu(T_{\rm e}, \boldsymbol{r})\rangle$ the mean scattering cross section averaged over the electron velocity distribution of temperature T_e at the position $\boldsymbol{r}$. To compute the mean cross section we use the Compton cross section given by the Klein-Nishina formula

$$\sigma(\hat{x}) = \tag{22}$$
$$= 2\pi r_{\rm e}^2 \frac{1}{\hat{x}}\left[(1-\frac{4}{\hat{x}}-\frac{8}{\hat{x}^2}\ln(1+\hat{x})+\frac{1}{2}+\frac{8}{\hat{x}}-\frac{1}{2(1+\hat{x}^2)}\right]$$

where

$$\frac{\hat{x}}{2} = \frac{h\nu}{m_{\rm e}c^2}\,\gamma\,(1-\boldsymbol{v}\cdot\boldsymbol{\Omega}/c). \tag{23}$$

Here $\boldsymbol{\Omega}$ denotes the direction of the photon, $\boldsymbol{v}$ the velocity of the electron, γ is the Lorenz factor and $r_{\rm e}$ is the classical electron radius.

Now we follow the photon trajectory form the moment of emission until the photon leaves the slab at the upper/lower boundary. The probability that the photon leaves unscattered is

$$P_i = \exp(-\tau_\nu), \tag{24}$$

where the index $i = 0, 1, 2,...$ denotes succeeding scatterings. The quantity $w_i P_i$ of the i-th scattering represents the transmitted fraction of the photon and is recorded to calculate the escape spectra. The portion $w_{i+1} = w_i(1-P_i)$ of the photon remains in the slab and undergoes the i+1-th scattering. The location where the photon scatters is determined by a random number. The velocity of the scattering electron is modeled by a relativistic Maxwell distribution corresponding to the temperature at the scattering position. We follow the photons until w becomes smaller than a certain minimum value $w_{\rm min}$. For the calculations reported here we use 60000 photons and $w_{\rm min} = 10^{-7}$.

The process of scattering is also calculated by the Monte Carlo method described in Podznyakov et al. (1983). The photon energy $h\nu'$ after a scattering is given by

$$h\nu' = \frac{h\nu(1-\boldsymbol{v}\cdot\boldsymbol{\Omega}/c)}{1-\boldsymbol{v}\cdot\boldsymbol{\Omega'}/c+\frac{h\nu}{\gamma m_{\rm e}c^2}(1-\boldsymbol{\Omega}\cdot\boldsymbol{\Omega'})}. \tag{25}$$

Thus we obtain the change of energy of an electron in its reference frame through scattering with a photon of weight w_i by

$$\mathrm{d}E_{\rm e} = w_i(h\nu' - h\nu) \tag{26}$$

at a position τ_i, where the scattering takes place. By recording the positions and energy differences of all scatterings of every photon we can calculate the electron cooling rates $f_{\rm c}^{-}(\tau)$ within the slab.

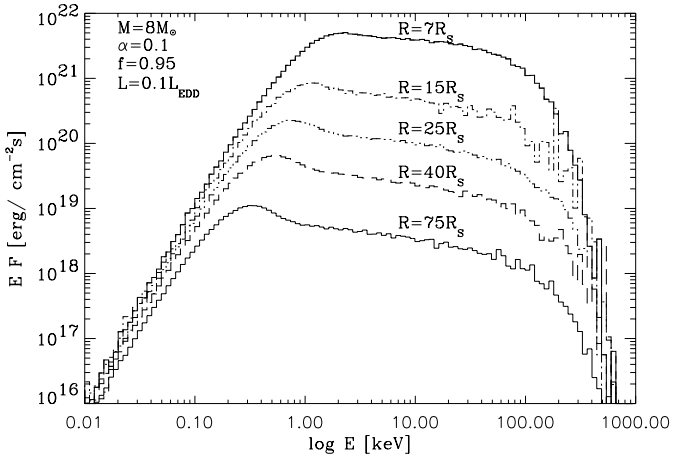

Fig. 4. Dependence of the spectrum on the distance from the compact object for a galactic BH with $M = 8M_\odot$. The spectra become slightly softer with increasing radius as the optical depth of the heated scattering layer gets smaller.

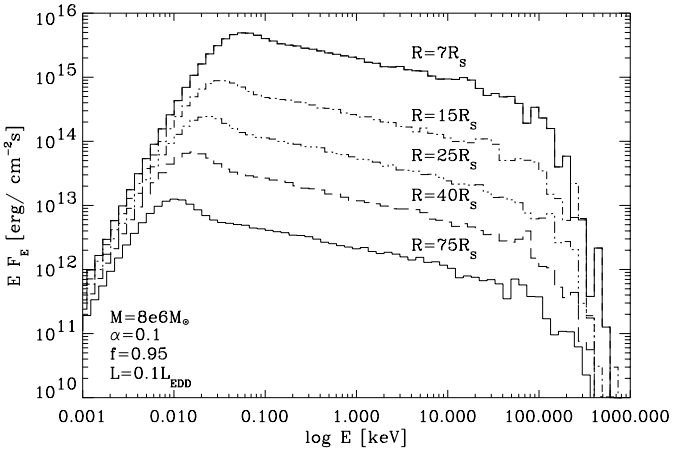

Fig. 5. Dependence of the spectrum on the distance from the compact object for an AGN with $M = 8 \times 10^6 M_\odot$ for $r = 7, 15, 25, 40$. Spectra in the AGN case are softer compared to the galactic BH spectra as the optical depth of the scattering layer is smaller.

3.3. Energy balance from heating and cooling

We start our calculations with an isothermal slab in hydrostatic equilibrium according to Sect. 2.1 and 2.2. After each Comptonization step we obtain the heating and cooling rates $f_{\rm p}^+(\tau)$ and $f_{\rm c}^-(\tau)$ within the slab. The time step in our simulation is adjusted to the shortest energy exchange time scale occurring in the calculation. The energy change (in erg cm^{-3}) after the time step Δt is then

$$\Delta E(\tau) = [f_{\rm p}^+(\tau) + f_{\rm c}^-(\tau)]\Delta t \tag{27}$$

Since heating or cooling of the layer takes place approximately isobarically the temperature change due to ΔE is

$$\Delta T_{\rm e}(\tau) = \frac{\Delta E(\tau)}{w(\tau)} T_{\rm e}(\tau) \tag{28}$$

where $w = \frac{5}{2}P$ is the enthalpy. With the new temperature profile we can update the hydrostatic disk structure after Eq. 14 and start a new heating/cooling step. After about 200 iterations we obtain an equilibrium state where the Coulomb heating is balanced by the Compton cooling and the temperature and density structure as well as the spectra have reached a stationary state.

4. Results from the model computations

For our model computations we use fixed values for the the accretion luminosity, the viscosity parameter of the cool disk, and the fraction of energy released in the corona, $L = 0.1L_{\rm Edd}$, $\alpha = 0.1$ and $f = 0.95$, respectively. We choose a galactic BH case with $M_{\rm BH} = 8M_\odot$ and an AGN case with $M_{\rm AGN} = 8 \times 10^6 M_\odot$. The thermalization depth is calculated according to Sect. 3.2.

Fig. 3 shows the spectra resulting when a fixed value of the thermalization depth is assumed. For $\tau_{\rm b} \approx 1$ the spectrum shows a prominent signature of soft photons, which cross the heated layer without scattering. Increasing the thermalization depth reduces the probability for the soft photons to leave the slab unscattered, and the spectra become harder. Thus the general shape of the emergent spectra is influenced by the depth of the thermalization layer.

If, instead of fixing the depth of the thermalizing boundary, its depth is adjusted such that the free-free emission of the layer matches the downward flux of hard photons to be thermalized (see Sect. 3.2), the spectra only depend on the energy input rate and the distance from the central mass. The temperature profiles through the proton heated layers are shown in Figs. 6 and 7. The thermalization depth $\tau_{\rm b}$ turns out to be located just below the largest depth to which the protons penetrate (seen as the slight kink above $\tau_{\rm b}$). This is because the free-free emissivity increases rapidly towards the base of the layer, where the density increases as $1/T$. The shape of the temperature profile is different from that in Spruit (1997) and Spruit & Haardt (2000), where the proton heating was treated more crudely as constant with depth.

Fig. 8 shows the dependence of the depth of the thermalization layer with increasing distance from the compact object for the galactic BH and the AGN cases. With increasing distance the thermalization depth moves closer to the disk surface, i.e. the Thomson depth of the Comptonizing layer is reduced. This is a consequence of the energy dependence of the proton penetration depth. With distance, the proton temperature, the penetration depth, and thereby the thermalization depth decrease. The effect of this distance dependence on the spectra is seen in Figs. 4, 5. At larger radii the spectra become slightly softer and the contribution of the unscattered soft photons becomes stronger. The AGN spectra are softer than the galactic BH spectra, and the cutoff energy increases slightly with distance from the central mass.

5. Discussion and conclusions

We have considered a model for the X-ray emission from an accretion disk illuminated by virialized protons from an ion

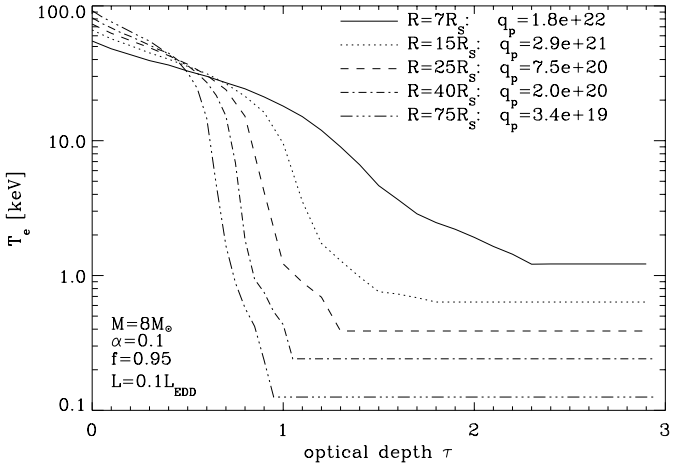

Fig. 6. Temperature profile as a function of optical depth in the electron scattering layer heated by the virialized protons for five different distances from a galactic BH. With increasing distance from the BH the penetration depth of the protons decreases and the surface temperature of the disk increases.

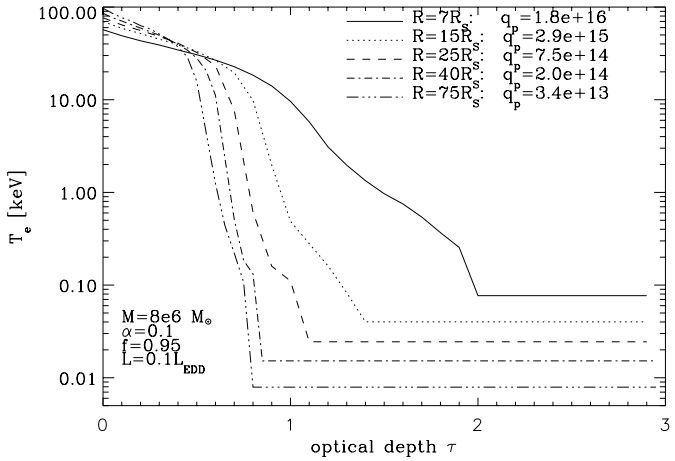

Fig. 7. Temperature profile as a function of optical depth in the electron scattering layer heated by the virialized protons for five different distances from an AGN.

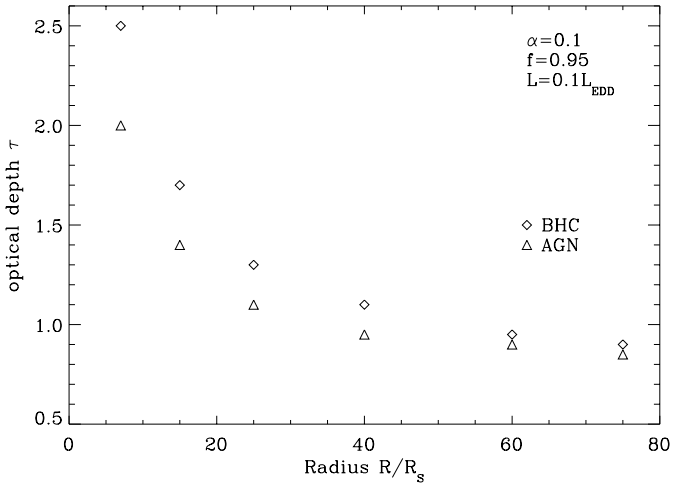

Fig. 8. Depth of the thermalization layer $\tau_{\rm b}$ as a function of distance from the central object for galactic BH case (diamonds) and AGN case (triangles). The thermalization depth is larger for the galactic black hole.

Table 1. Compton y–parameter of the proton heated layer in the galactic BH case. $\tau_{\rm b}$ is the Thomson depth of the layer as a function of distance.

$R/R_{\rm S}$	7	15	25	40	60	75
$\tau_{\rm b}$	2.50	1.70	1.30	1.10	0.95	0.90
y	0.43	0.43	0.43	0.41	0.41	0.42

supported torus or an ADAF. This situation may arise in the transition region between a cool disk and an ADAF, or in cases where a cool disk survives to some distance inside an ADAF. Another possibility might be a magnetic flare-heated disk corona (e.g. di Matteo et al. 1999), if ions are heated there to values near the virial temperature.

For definiteness of the model, we have assumed that the dissipation of gravitational energy mainly takes place in the ADAF or corona which supplies the hot ions, and only a small fraction of the gravitational energy is released in the cool disk that acts as target.

The heating of the cool disk by the protons produces X-ray spectra that are very reminiscent of the hard spectra of accreting galactic black holes and AGN. The spectra have a power law slope in $EF(E)$ with spectral index $s \approx 0.2$ in the galactic BH case and $s \approx 0.3$ in the AGN case. There are only small deviations between the spectra depending on the distance from the hole and the mass of the hole.

The constancy of the spectral slope can be traced to two factors. One is the Haardt-Maraschi regulating mechanism. By the energy balance of the Comptonizing layer, the contributions of the soft and hard photons to the luminosity adjust to become roughly equal. The spectra still depend on the assumed thermalization depth, however, as seen in Fig. 3. To get an approximate fix for this depth, we have adjusted it such that the free-free emission from the layer matches the downward flux of photons at the base of the layer. With this approximation, the thermalization depth closely tracks the maximum penetration depth of the ions, so that the Comptonization conditions are quite similar in all cases. This further increases the similarity of the spectra. This similarity can be checked also by computing, as an approximate indicator of the degree of Comptonization, a generalized Compton-y parameter. Since the temperature varies through the Comptonizing layer, we measure this by the quantity

$$y = \int_0^{\tau_{\rm b}} (4\Theta + 16\Theta^2)\,{\rm d}\tau, \qquad (29)$$

where Θ is the local disk temperature in units of the electron rest mass, $\Theta = k_{\rm B}T_{\rm e}(\tau)/m_{\rm e}c^2$. Some values are shown in Table 1. This Compton y–parameter is of the order 0.4 and does not change significantly with distance r from the central object. In the model of Haardt & Maraschi (1993) y was of order 0.6.

The main difference between the spectra are the soft photon energy (the shoulder at the left side in Figs. 4 and 5), which increases with luminosity, and the high-energy cutoff. The cutoff is seen to increase slightly with distance from the central mass. This can be traced to the fact that with increasing distance the temperatures at the top of the Comptonizing layer increase somewhat (though the average temperature, proportional to y, is nearly constant). This somewhat increases the flux of photons at the highest energies.

A questions unanswered by the present results is of course whether a significant region of interaction between a hot ion plasma and a cool disk can exist. Since the cool disk absorbs all incident ions, the cool disk is a strong sink of both mass and energy for the hot ion plasma. A second question relates to the thermalization of the downward flux of energetic photons in the cool disk. As our results show, the slope of the resulting X-ray spectrum depends somewhat on the effective depth of thermalization of these photons. A correct treatment of the thermalization requires detailed consideration of the contributing atomic processes (Matt et al. 1993).

Acknowledgements. We thank the referee Roberto Turolla for his fast response and valuable remarks on the paper.

This work was done in the research network "Accretion onto black holes, compact stars and protostars" funded by the European Commission under contract number ERBFMRX-CT98-0195

References

Alme M.L., Wilson J.R., 1973, ApJ 186, 1015
di Matteo T., Celotti A., Fabian A.C., 1999, MNRAS 304, 809
Galeev A.A., Rosner R., Vaiana G.S., 1979, ApJ 229, 318
Haardt F., Maraschi L., 1991, ApJ Lett. 380, L51
Haardt F., Maraschi L., 1993, ApJ 413, 507
Matt G., Fabian A.C., Ross R.R., 1993, MNRAS 264, 839
Narayan R., McClintock J.E., Yi I., 1996, ApJ 457, 821
Narayan R., Yi I., 1994, ApJ Lett. 428, L13
Narayan R., Yi I., 1995, ApJ 444, 231
Pozdnyakov L.A., Sobel I.M., Syunyaev R.A., 1983, Astrophysics and Space Physics Research 2, 189
Rees M.J., Phinney E.S., Begelman M.C., Blandford R.D., 1982, Nat 295, 17
Rutledge R.E., Lewin W.H.G., van Der Klis, et al., 1999, ApJS 124, 265
Rybicki G.B., Lightman A.P., 1979, Radiative processes in astrophysics, Wiley-Interscience, New York
Ryter C., Reeves H., Gradsztajn E., Audouze J., 1970, A&A 8, 389
Shakura N.I., Sunyaev R.A., 1973, A&A 24, 337
Shapiro S.L., Lightman A.P., Eardley D.M., 1976, ApJ 204, 187
Spitzer L., 1962, Physics of fully ionized gases, Wiley, New York
Spruit H.C., 1997, in Berlin Springer Verlag Lecture Notes in Physics, Vol. 487, pp 67–76
Spruit H.C., Haardt F., 2000, MNRAS submitted
Svensson R., Zdziarski A.A., 1994, ApJ 436, 599
Zel'dovitch Y.B., Shakura N.I., 1969, Soviet Astron.-AJ 13, 175